JOURNAL OF MATERIALS SCIENCE 32 (1997) 3207–3212

Sintering of injection-moulded WC–7 wt % Ni in a hydrogen atmosphere

CHENG LIANG
Materials and Mineral Resources Engineering Department, National Taipei Institute of Technology, Taipei, Taiwan

SHUN-TIAN LIN*
Mechanical Engineering Department, National Taiwan Institute of Technology, Taipei, Taiwan

Sintering injection-moulded WC–7 wt % Ni in a hydrogen atmosphere at temperatures higher than 900 °C resulted in an inhomogeneous microstructure, as Ni_2W_4C (η phase) preferentially developed near the surface of specimens. Subsequent to sintering at temperatures higher than the liquid-phase formation temperature, the surface of specimens was virtually composed of η phase. This arose from the excessive decarburization occurring near the surface of specimens, and the exudation of the Ni-based metal binder towards the surface of specimens. Primarily caused by the dissolution of W into the Ni binder phase, the saturation magnetization of WC–7 wt % Ni decreased at temperatures lower than 1000 °C.

1. Introduction

Powder injection moulding (PIM) is a process route capable of mass producing high-performance and complex-shaped components [1]. This process proves cost effective in producing components that require intensive secondary operations. The benefits of adopting PIM as the manufacturing route are especially obvious when the materials to be fabricated are hard to machine, such as cemented carbides. Nevertheless, a major issue which remains to be resolved for the injection moulding of cemented carbides is control of the carbon content. The binder used in injection moulding, which usually constitutes about 50 vol % of the green parts, contains certain fractions of high-molecular-weight polymers. Depending on the debinding conditions, pyrolysis of the binder can result in various degrees of carbon contamination in the injection-moulded components [2]. Thus, compared with die pressing or cold isostatic pressing, PIM requires a slightly different approach to control of the carbon content. Decarburization is usually carried out in the binder burn-out cycle to get rid of the contamination of excess carbon resulting from incomplete binder pyrolysis. However, excessive decarburization is also detrimental to the properties. The pyrolysed polymers are much more difficult to collect in the binder condenser than in the paraffin wax used in die pressing or cold isostatic pressing. It is thus preferable to debind and sinter the injection-moulded components in separate furnaces to avoid the batch-to-batch cross-contamination. Consequently, pre-sintering should be carried out in the debinding cycle to impart strength to the debound parts.

Cemented carbides are usually densified by liquid-phase sintering. The densification stages of the classical persistent liquid-phase sintering model include the sequential events of rearrangement of particles, solution and precipitation of the particles, and solid-phase sintering of the particles [3]. In addition to these three stages, solid-state sintering prior to the formation of eutectic liquid phase can result in various degrees of densification [4]. The relative contribution from each stage depends on the processing conditions and materials characteristics. For example, WC–6% Co could be sintered to more than 90% of the theoretical density at temperatures lower than the eutectic temperature, which thus eliminated the rearrangement of particles subsequent to the formation of the eutectic phase [3]. On the other hand, the rearrangement of WC particles was effective in sintering of WC–12 wt % Ni, even though a sintered density higher than 85% of the theoretical density had been achieved prior to the formation of the eutectic liquid phase [5].

The goal of this research was to investigate the sequential stages involved in the sintering of injection-moulded WC–7 wt % Ni in a hydrogen atmosphere. Hydrogen was utilized because it is a strong reducing atmosphere which not only protects the alloys from oxidation but also effectively reduces the contamination of carbon arising from incomplete binder burn-out [2]. The variations in physical properties were examined and correlated with the evolution of the microstructure.

*Author to whom all correspondence should be addressed.

0022–2461

2. Experimental procedures

The material used in this study was WC–7% Ni. Some characteristics of the powders are shown in Table I. The initial carbon content and the stoichiometric carbon content of the powder mixture were 5.72 wt %, and 5.70 wt %, respectively. The powders were loaded in a plastic jar and wet milled in heptane for 24 h. The load in the plastic jar was composed of 14 vol % powder, 38 vol % heptane and 48 vol % type 304 stainless steel balls with a diameter of 3 mm. After milling, the powder–solvent paste was separated from the stainless steel balls by screening, and this was followed by drying at 80 °C for 8 h. The binder was composed of polypropylene (20 wt %), ethylene vinyl acetate (25 wt %), paraffin wax (50 wt %) and stearic acid (5 wt %). The powder–binder mixture, which had a powder volume fraction of 0.5, was prepared using a *Z*-blade mixer at 190 °C for about 90 min. Rectangular test specimens having dimensions of 70 mm × 12 mm × 4 mm were molded using a reciprocating-screw injection moulding machine.

The moulded specimens were immersed in heptane to remove paraffin wax and stearic acid partially, which reduced the possibility of forming defects in the subsequent thermal debinding. Because of the relatively small quantity of specimens compared with the furnace volume and gas purging rate, thermal debinding and sintering were carried out in a single batch using a horizontal tube furnace. The thermal profile was as follows: heating to 300 °C at a rate of 3 K min^{-1} and holding for 30 min; then heating to 500 °C at a rate of 3 K min^{-1}, and holding for 1 h; finally heating to the sintering temperature at a rate of 10 K min^{-1} and holding for 1 h. Sintering temperatures from 600 to 1600 °C were investigated. A dry hydrogen atmosphere (dew point, − 30 °C) was used in the thermal processing.

Scanning electron microscopy (Cambridge S360) was used for morphological analysis. Phase analysis of the bulk sintered specimens was carried out using an X-ray diffractometer (Rigaku D Max B) with Cu Kα radiation at an accelerating voltage of 40 keV. Microanalysis of the morphology, composition and structure of the matrix phase was conducted using scanning transmission electron microscopy (STEM) (JEOL 2000 FX) at an accelerating voltage of 200 keV. Energy-dispersive X-ray analysis (EDXA) spectra and selective-area electron diffraction patterns were recorded for chemical composition and structure analysis. The specimens for STEM were prepared by mechanically grinding to a thickness of about 0.5 mm, dimple grinding to a thickness of about 15 μm and then using ion beam milling until perforation. Magnetic saturation measurement was conducted using a magnetic hysteresis loop tracer. The transverse rupture strength was measured by four-point bending tests. The gap length between two adjacent points was 10 mm. The carbon content of each specimen was measured using the combustion method (Leco CS-224). The samples for carbon analysis were taken from near the surface of the sintered specimens. All the reported data were the average of at least three test results.

TABLE I Characteristics of WC and Ni powders

Powder	WC	Ni
Vendor	Korea Tungsten	Novamet
Grade	KC-0	Inco 123
Mean particle size (μm)	2.2	9.8
Major constituents (wt %)	C, 6.14	O, 0.15
	Fe, 0.02	C, 0.10
	Co, 0.01	Fe, 0.01
	W, balance	Ni, balance

3. Results and discussion

Fig. 1 shows the sequential phase evolution with the increase in sintering temperature for the locations near the surface and core of specimens. Severe phase transformation took place near the surface of specimens at 900 °C, above which the formation of η phase became significant. The diffraction peaks of Ni for the surface of specimens virtually disappeared with the formation of η phase. Additionally, the relative abundance of the η phase increased at the expense of WC. Eventually, the surface of specimens was essentially composed of η phase at temperatures higher than the eutectic temperature of WC–Ni (1342 °C) [6]. On the other hand, the core of specimens was virtually not affected in increase in the sintering temperature. Thus, microstructural inhomogeneity developed in the specimens, caused by the gradual decarburization from the surface towards the core of specimens by the hydrogen atmosphere [2].

Fig. 2 shows the microstructural evolution near the core of specimens sintered at temperatures ranging from 600 to 1500 °C. The large isolated Ni particles could still be observed at sintering temperatures as high as 800 °C but could not be found at sintering temperatures higher than 900 °C. Additionally, there was no substantial increase in grain size of WC or sintered density with the disappearance of isolated Ni grains. Thus, intensive diffusion of Ni towards the contact regions of WC grains took place at 900 °C, which subsequently formed the pendular bonds between WC grains. Since Ni has a very low solubility in WC [6], the mass transfer mechanism of Ni towards the contact regions of WC grains was obviously through diffusion of Ni atoms on the surface of WC grains. The densification rate and grain growth rate of WC phase were raised owing to the existence of pendular bonds between WC grains, which can be observed in Fig. 2(e). The loosely packed region with clusters of larger WC grains for the specimen sintered at 1100 °C was a result of enhanced mass transfer of WC through the pendular bonds. However, no substantially abnormal grain growth occurred, even at a sintering temperature of 1500 °C. Most of the WC grains were smaller than 1 μm with a few grains larger than 2 μm.

Fig. 3 shows the transmission electron micrographs and selected-area electron diffraction pattern for a specimen sintered at 1430 °C. The domain, which looked like a single large grain in the bright-field

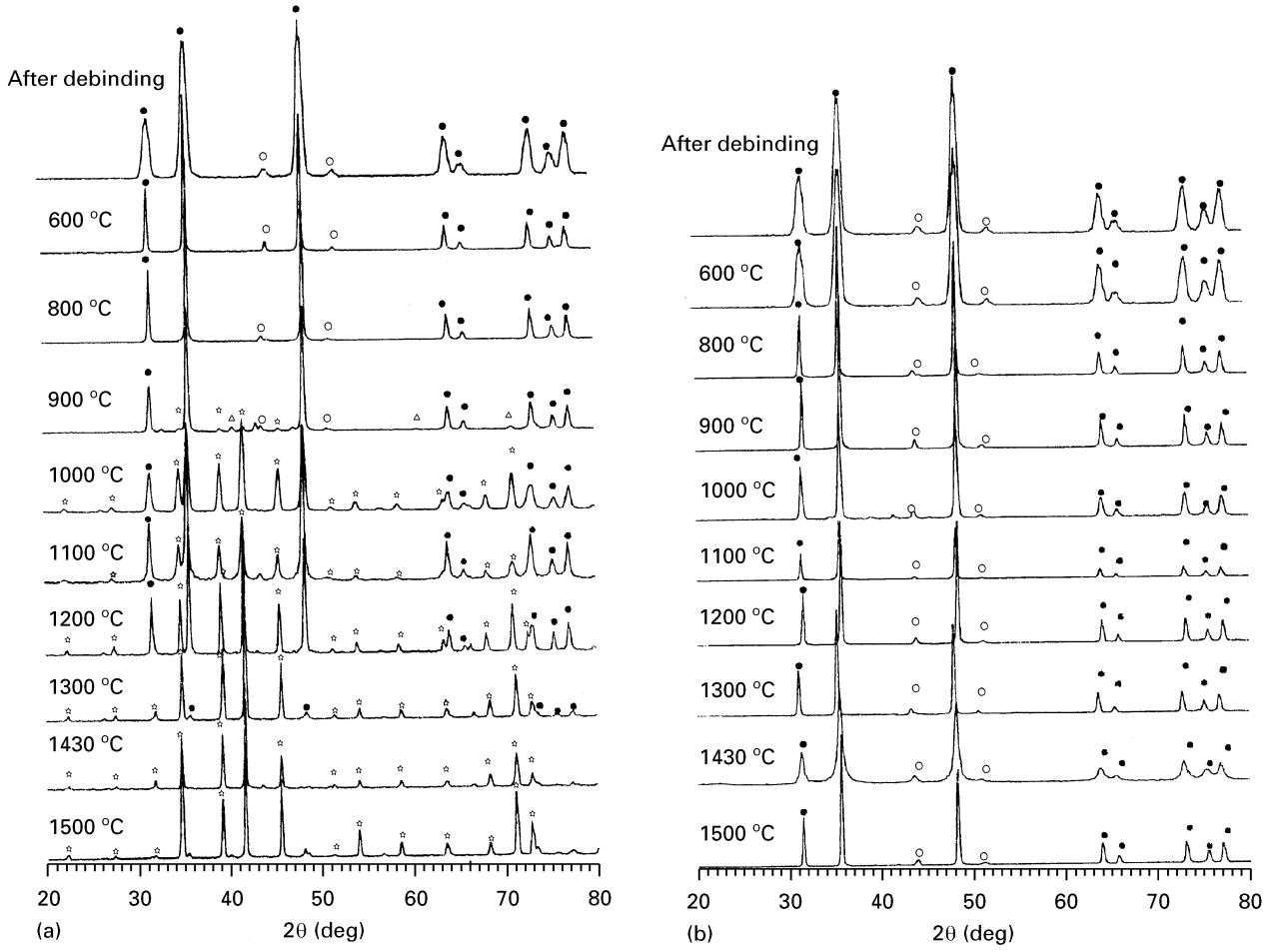

Figure 1 X-ray diffraction patterns for (a) the surface and (b) the core of specimens sintered at various temperatures. (●), WC; (○), Ni; (☆), Ni_2W_4C; (△), W_2C.

image, was composed of very fine precipitates, as seen in the dark-field image. The selected-area electron diffraction pattern further confirmed the existence of fine precipitates in this domain. This ring pattern indicated that the single domain observed in the bright-field image was composed of nanocrystalline grains that had no preferred orientation. The structure of the nanocrystalline grains was determined to be cubic and the lattice parameter to be 1.125 nm. Additional composition analysis based on EDXA indicated that these nanocrystalline grains were composed of η phase. In comparison, unidentified fine-grained precipitates having an average grain size of about 10 nm were found in the WC–Ni-based cemented carbides [7].

The existence of uniformly distributed nanocrystalline grains of η phase in the domain indicated that the distributions of Ni, W and C in the domain were very homogeneous prior to the crystallization of the η phase. Thus, these nanocrystalline grains of η phase were induced by the abrupt transformation from liquid phase into solid phase upon cooling. Similarly, transformation from liquid phase into solid phase upon cooling caused the coprecipitation of WC and η phase in a single grain, when the concentration of Ni was lower in the liquid prior to transformation. Fig. 4 shows the bright-field image and selective-area electron diffraction pattern for a specimen sintered at 1430 °C. As can be seen in the diffraction pattern, the spots with weaker intensities (cubic; $a = 1.125$ nm) orderly overlapped with the diffraction spots of hexagonal WC phase ($a = 0.2906$ nm; $c = 0.2838$ nm). The grains composed of coherent WC and η phase were so abundant that about one fifth of the diffraction patterns examined in this study were similar to that shown in Fig. 4. In comparison, a coherent nanocrystalline phase precipitating from WC phase was found in a carbon-deficient WC–10 wt % Ni, whose structure was postulated to be NiW [8].

Fig. 5 shows the variations in sintered density, total carbon content for locations near the surface of specimens, saturation magnetization and transverse rupture strength with sintering temperature. The increase in strength became evident at the sintering temperature of 900 °C, as a result of the formation of pendular bonds between WC grains. A further increase in strength, accompanied by an increase in density, was attributed to the enhanced diffusivity of WC through the Ni phase. However, the plateau strength achieved in this study was pretty low, owing to the formation of excessive η phase near the surface of specimens. The ductile nickel phase was consumed as a result of the formation of η phase, which caused the specimens to behave more or less like ceramic materials with very low transverse rupture strengths. Although with relatively low transverse rupture strengths, the specimens sintered at 1430 °C still had a mean Rockwell A hardness of 87 HRA. The total carbon content near the

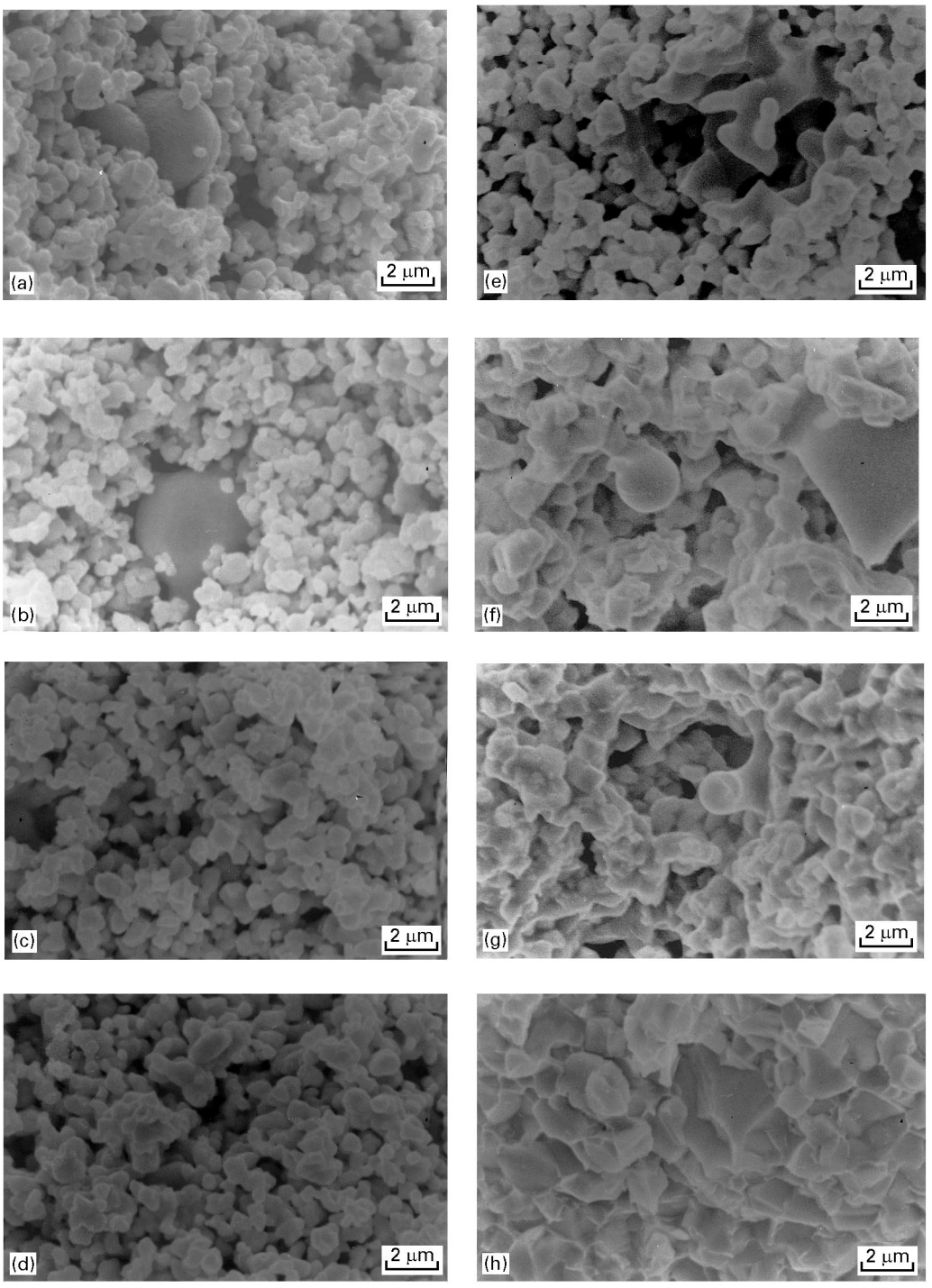

Figure 2 Microstructures of specimens sintered at (a) 600 °C, (b) 800 °C, (c) 900 °C, (d) 1000 °C, (e) 1100 °C, (f) 1200 °C, (g) 1300 °C, and (h) 1500 °C.

surface of specimens and saturation magnetization decreased with increase in sintering temperature. The total carbon content near the surface of specimens after sintering at 600 °C was about 0.25 wt % higher than the carbon content of the initial powder mixture (5.72 wt %). Further decarburization should be carried out at higher temperatures in order to maintain a carbon content near the stoichiometric level. The stoichiometric carbon content was achieved at approximately 900 °C, at which a very low green strength was attained.

The most pronounced observation was that the saturation magnetization dropped very rapidly from 600 to 800 °C and reached almost zero at 1000 °C. The decrease in the saturation magnetization was caused by the dissolution of W and C atoms into the Ni phase [6, 8]. In fact, the dissolution of W into Ni has a greater effect on the reduction of saturation magnetization than the dissolution of C into Ni [6]. For example, the solubility of C in Ni is low (less than 1 wt %) that the dissolution of 0.4 wt % C into Ni caused a decrease of only 6% in saturation magnetization [9]. On the other hand, the solubility of W in Ni is about 20 wt %; the dissolution of 16 wt % W into Ni caused a decrease of about 77% in the saturation magnetization [9]. Since the dissolution of W into Ni

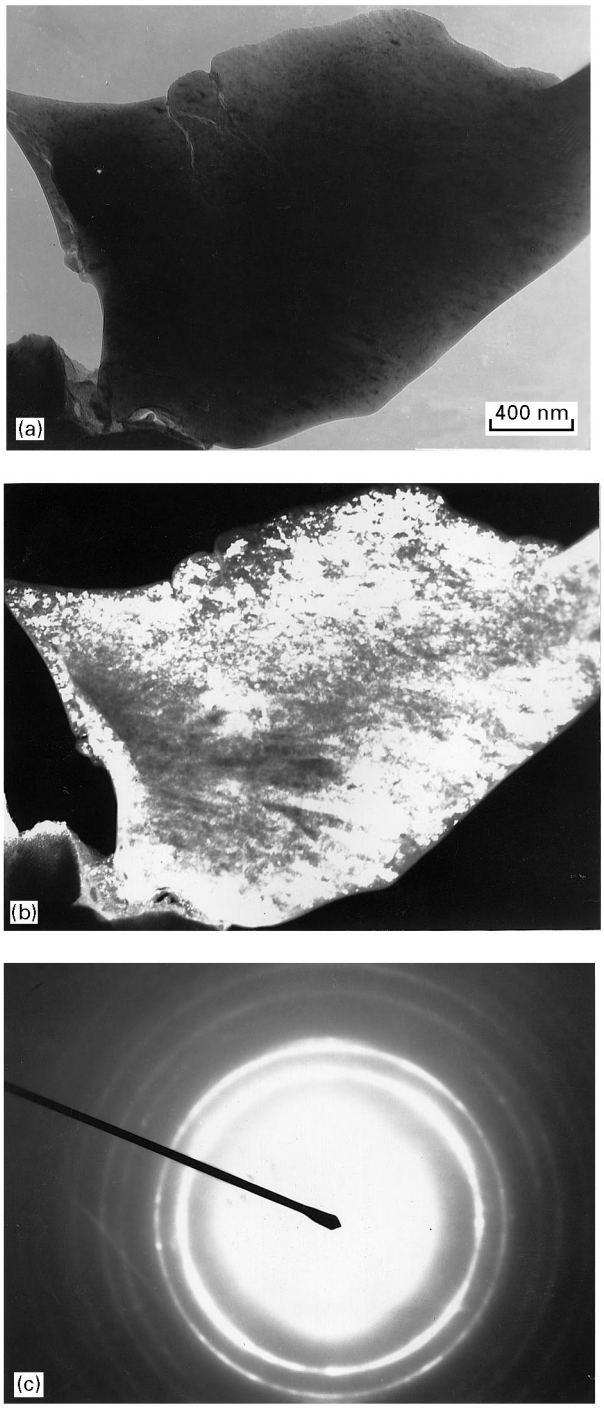

Figure 3 (a) Bright-field transmission electron micrograph, (b) dark-field transmission electron micrograph, and (c) selected-area electron diffraction pattern, for a specimen sintered at 1430 °C.

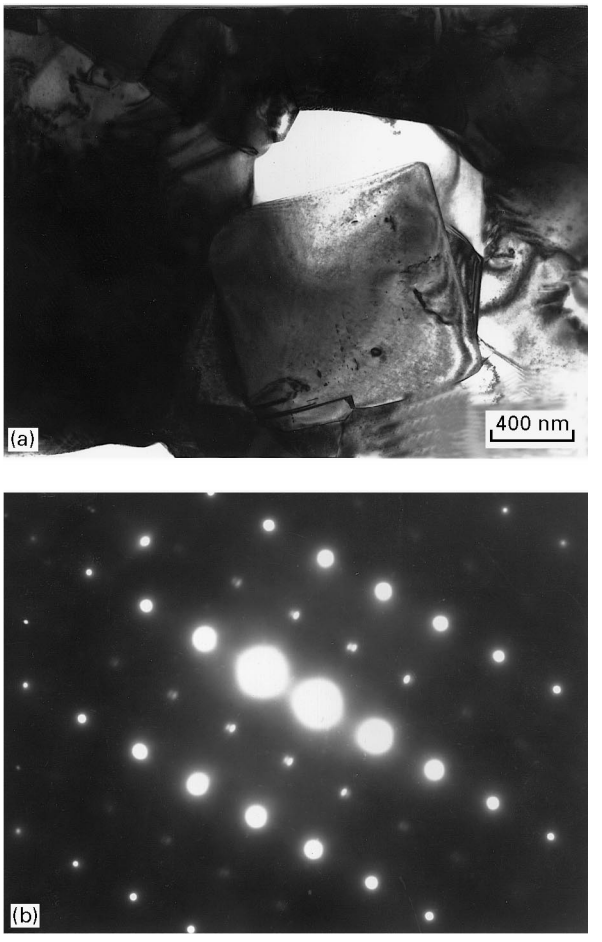

Figure 4 (a) Bright field transmission electron micrograph and (b) selected-area electron diffraction pattern along the $\langle 1\,0\,1\,0 \rangle$ zone axis of WC and the $\langle 2\,0\,0 \rangle$ zone axis of Ni_2W_4C for a specimen sintered at 1430 °C.

is retarded by the interstitial dissolution of C in Ni, the decrease in carbon content at temperatures between 600 and 800 °C could have reduced the saturation magnetization of the alloy by increasing the solubility of W in Ni [8]. Loss of the saturation magnetization of cemented carbides is believed to be caused by the loss of the metal binder phase arising from the formation of η phase [10]. Such a suggestion was ruled out in this work as there was no phase transformation prior to the loss of saturation magnetization at temperatures lower than 900 °C (Fig. 1). Additionally, the total carbon contents at temperatures lower than 900 °C were higher than the stoichiometric carbon

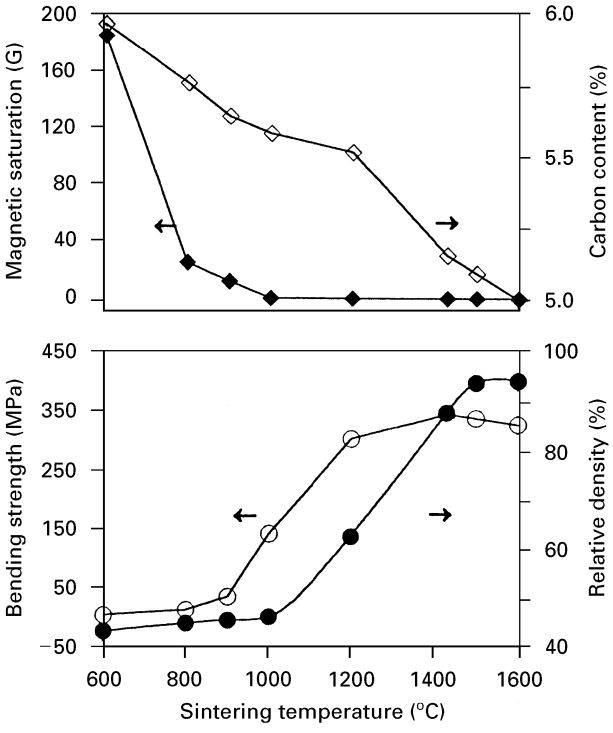

Figure 5 Variations in sintered density, total carbon content near the surface of specimen, saturation magnetization and transverse rupture strength with sintering temperature.

content (5.70 wt %) that formation of the η phase was less possible.

The predominant formation of the η phase near the surface of specimens was caused not only by the loss of carbon during sintering but also by the exudation of liquid phase that was rich in Ni from the core to the surface of specimens. This argument was assumed by comparing the molar ratios of Ni, W and C for the starting powder and η phase. The molar ratio of Ni, W and C for the starting powder was approximately 1:4:4 while that for η carbide was 2:4:1. The alteration of the molar ratio of these three elements subsequent to sintering suggested that carbon must have been removed from the surface while Ni must have been supplied to the surface to fulfil the requirement of stoichiometry. Consequently, exudation of the liquid phase from the core to the surface of specimens occurred during sintering, a result caused by the rearrangement of particles subsequent to the formation of liquid phase.

4. Conclusion

The binder burn-out residue of injection-moulded WC–7 wt %Ni could be effectively eliminated by reducing the residue in hydrogen. However, excessive decarburization took place when the sintering temperature was too high. Decarburization initiated from the surface into the core of specimens, which developed a concentration gradient of carbon in the specimens and facilitated the predominant formation of η phase near the surface of specimens. The inhomogeneous distribution of Ni in WC, owing to the larger particle size of Ni, resulted in non-uniform densification and grain growth of WC phase. The liquid phase formed at temperatures higher than the eutectic temperature was microscopically inhomogeneous in composition. Thus, upon cooling, part of the liquid phase precipitated into nanocrystalline grains of η phase or grains composed of coherent WC and η phase.

Acknowledgement

The work was financially supported by National Science Council, Taiwan, through Contract NSC 84-2216-E011-032.

References

1. R. M. GERMAN, "Powder injection molding" (Metal Powder Industries Federation, Princeton, NJ, 1990) p. 1.
2. Y. L. HO and S. T. LIN, *Metall. Mater. Trans. A* **25** (1995) 133.
3. R. M. GERMAN, "Liquid phase sintering" (Plenum, New York, 1985) pp. 1, 65.
4. R. M. GERMAN, S. FAROOQ and C. M. KIPPUT, *Mater. Sci. Engng.* **A105** (1988) p. 215.
5. W. J. HUPPMANN and G. PETZOW, "Modern developments in powder metallurgy," Vol. 9, edited by H. H. Hausner and P. V. Taubenblat (Metal Powder Industries Federation, Princeton, NJ, 1977) p. 77.
6. V. A. TRACEY, *Int. J. Refract. Metals Hard Mater.* **11** (1992) 137.
7. E. F. DRAKE and A. D. KRAWITZ, *Metall. Trans. A* **12** (1981) 505.
8. H. L. ROUX, *J. Mater. Sci.* **20** (1985) 407.
9. B. ROEBUCK, E. G. BENNETT and E. A. ALMOND, *Int. J. Refract. Metals Hard Mater.* **3** (1984) 35.
10. K. J. A. BROOKES, "Hardmetals and other hard materials" (International Carbide Data, East Barnet Herts., 1992) p. 92.

Received 25 March
and accepted 11 December 1996